

Electronic supporting Information

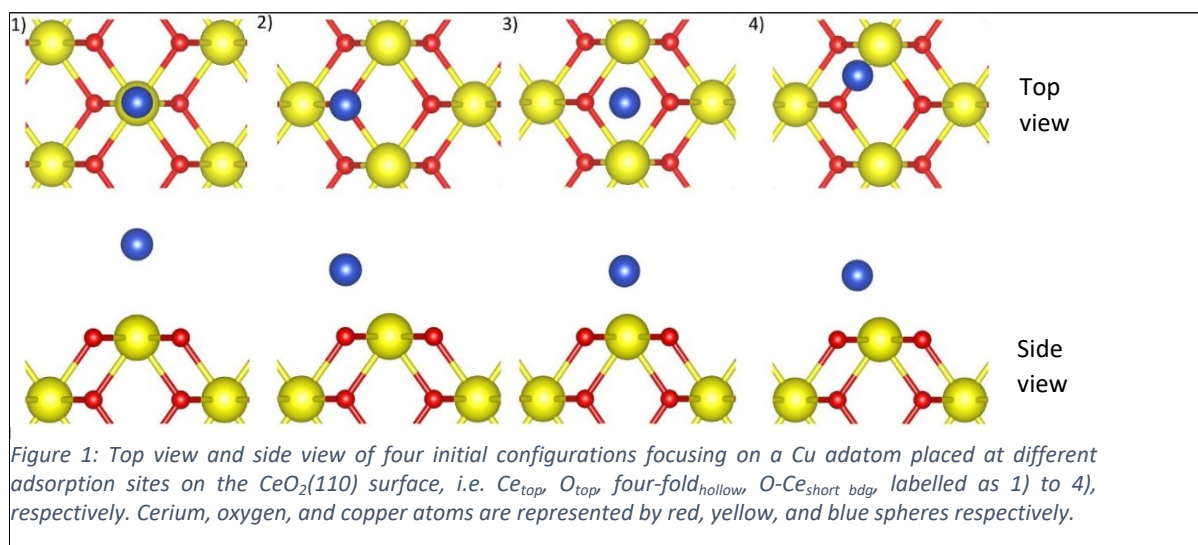
A computational investigation of the adsorption of small copper clusters on the CeO₂(110) surface

Rui Zhang^{(1)*}, Arunabhiram Chutia^{(2)*}, Alexey A. Sokol⁽³⁾, David Chadwick⁽¹⁾, C. Richard A. Catlow^{(3),(4)}

1. Dept of Chemical Engineering, Imperial College London, South Kensington Campus, London SW7 2AZ
2. School of Chemistry, University of Lincoln, Lincoln, LN6 7TS, UK
3. Dept of Chemistry, University College London, 20 Gordon St., London WC1 HOAJ
4. School of Chemistry, Cardiff University, Park Place, Cardiff CF10 1AT

1.1 Adsorption of Cu adatom on CeO₂(110) surface

A Cu adatom was initially placed at four different adsorption sites on the CeO₂(110) surface¹, *i.e.* on top of a surface Ce atom (Ce_{top}), a surface O atom (O_{top}), the middle of a surface four-fold hollow site (four-fold_{hollow}) and the middle of an O-Ce short bridge site (O-Ce_{short bdg}), as illustrated in ESI Fig. 1.



Local surface distortion around the Cu adatom is observed in the three optimised structures obtained from O_{top}, O-Ce_{short bdg}, and four-fold_{hollow}, respectively, as illustrated in ESI Fig. 2 2-4, also evidenced by the average surface Ce-O bond lengths different from that of a pristine surface, as listed in Table 1, with a negative adsorption energy of -3.258 eV, -3.165 eV, and -1.112 eV, respectively. O_{top} and O-Ce_{short bdg} show essentially the same optimised structures, *i.e.* the Cu atom is close to the surface, bonded with two surface O ions on top of a second-layer Ce ion (named as an O-Ce-O long bridge site), though they have different initial Cu positions. Both their optimised structures show, as noted, a very short Cu-O distance around 1.77 Å, indicating strong Cu-O interactions with the surface O ions. By investigating the partial density of states (PDOS) of the Cu adatom (4s, 3p and 3d) and its two bonded O ions (2s and 2p) of these two configurations, as illustrated in ESI Fig. 3, we found that the overlapping between Cu 3d and O 2p signatures in the ranges between -1 and 0 eV, and between -5.5 and -4.5 eV

is slightly stronger in the optimised structure of O_{top} than in that of $O-Ce_{short\ bdg}$, thus explaining the more negative adsorption energy of the former one ¹.

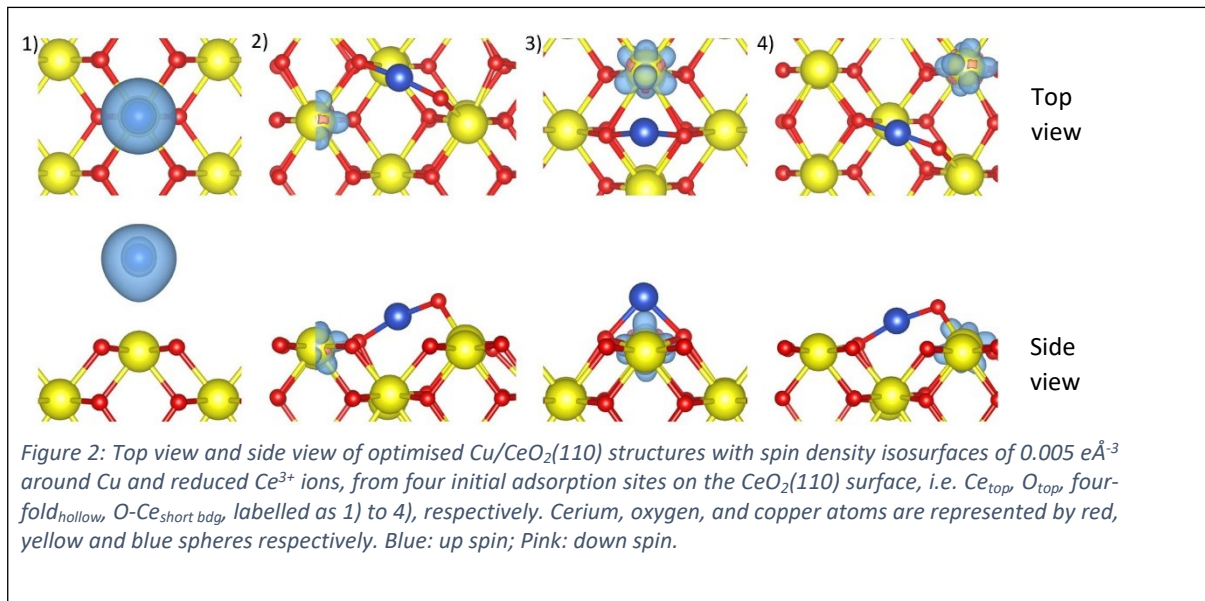
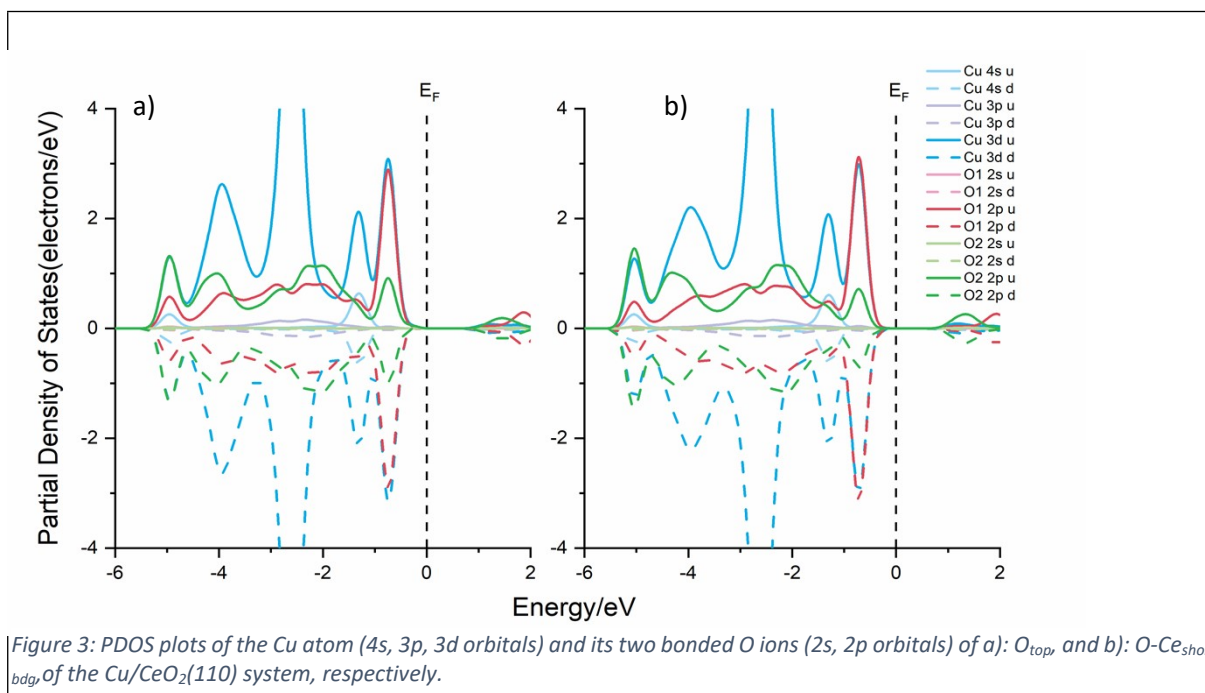


Table 1: Cu/CeO₂(110) system: calculated magnetic moment of Ce³⁺ ions (s, p, d, f orbitals) in Bohr magneton (μ_B); Cu-O bond length (Å) between Cu and the nearest surface O ion; average Ce-O bond length (Å) on the surface and in the two sublayers; adsorption energy per Cu atom (eV).

System	M_{Ce} (μ_B)	Cu-O (Å)	(Ce-O) _{surf} (Å)	(Ce-O) _{sub} (Å)	E_{ad} (eV)
Pristine	--	--	2.342	2.377	--
Ce _{top}	--	--	2.342	2.377	-0.326
O _{top}	0.967	1.771	2.343	2.376	-3.258
four-fold _{hollow}	0.950	1.959	2.353	2.385	-1.112
O-Ce _{short bdg}	0.966	1.765	2.333	2.381	-3.165



For the optimised structure of four-fold_{hollow}, the Cu atom stays close to its initial position, bonding with two surface O ions from the four-fold hollow site; because of its longer Cu-O distance and weaker Cu-O interactions, it shows a less negative adsorption energy, as compared to the aforementioned two. For the optimised structure of Ce_{top}, the Cu adatom hardly interacts with the surface (see ESI Fig. 2.1), showing a distance of 3.27 Å to the nearest surface Ce⁴⁺ ion¹; the weakest interaction between Cu and the ceria surface therefore leads to the least negative adsorption energy of -0.326 eV.

Considering now their electronic structures, in all configurations except Ce_{top} there is one electron transferred from the Cu to a surface Ce⁴⁺ ion, indicated by the excess spin density isosurfaces (see ESI Fig. 2) and the calculated magnetic moment of the reduced Ce³⁺ ions in the range of 0.95-0.97 μ_B (ESI Table 1). The reduced surface Ce³⁺ ion is a nearest neighbour to the Cu in the three configurations¹⁻², which in O_{top} however changes from the initial Ce³⁺ position set for geometry optimisation. There is clearly a flat energy surface for Cu adsorption on ceria, with many local minima, some of which being very close to the global minimum calculated in earlier work¹⁻², which explains a slightly more negative adsorption energy of O_{top} calculated in this work.

The electron transfer is also confirmed by a PDOS analysis. A Ce⁴⁺ ion typically shows no 4f orbital signatures just below the Fermi energy (E_F) (see ESI Fig. 4), whereas the reduced Ce³⁺ ion in O_{top} shows a distinct 4f signature just below E_F , indicating one electron gained in its 4f orbitals. Ce³⁺ 4f orbital PDOS plots of the other two configurations are essentially the same as that of O_{top}, which therefore are not presented here. For the Ce_{top} configuration, the electron remains in the Cu 4s orbital, as indicated by the Cu 4s orbital PDOS plot illustrated in ESI Fig. 5, which is similar to that of a single Cu in the gas phase (ESI Fig. 6).

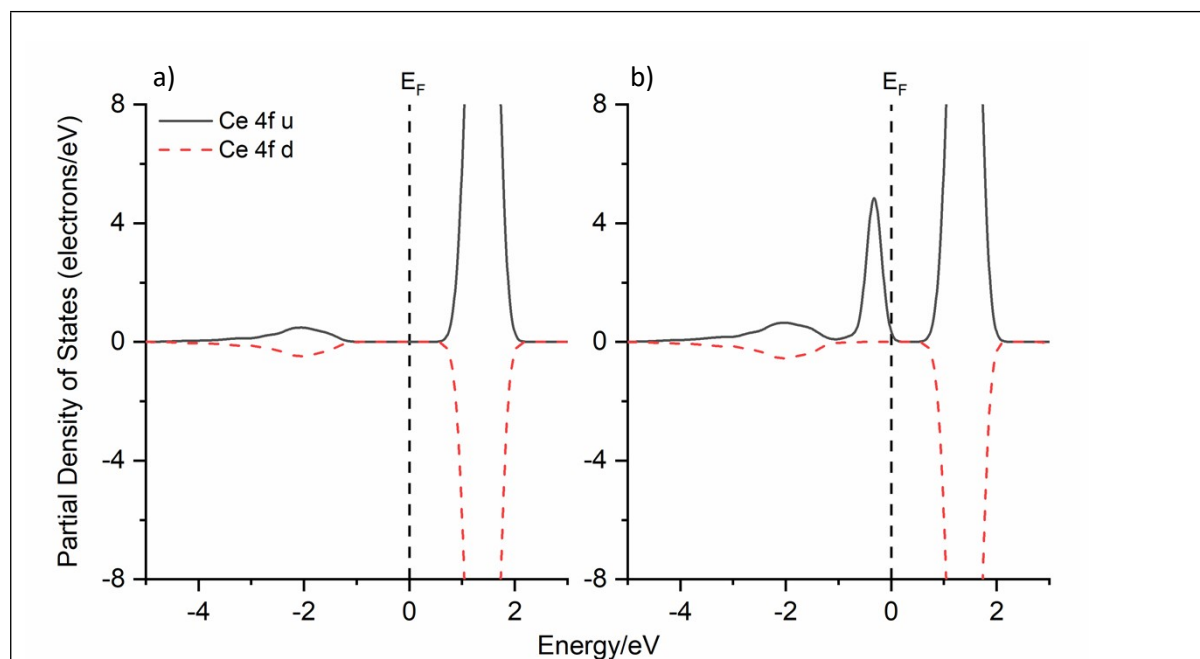
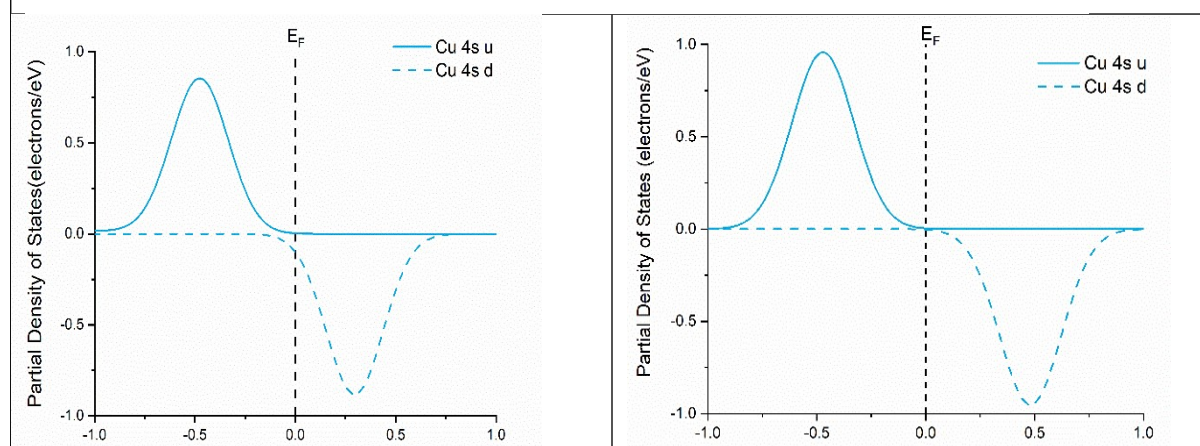


Figure 4: a) typical PDOS of Ce 4f orbitals of a Ce⁴⁺ ion in the fixed layers of a CeO₂(110) slab; b) PDOS of Ce 4f orbitals of the reduced Ce³⁺ ion in the structure optimised from O_{top}. u: up spin, d: down spin.



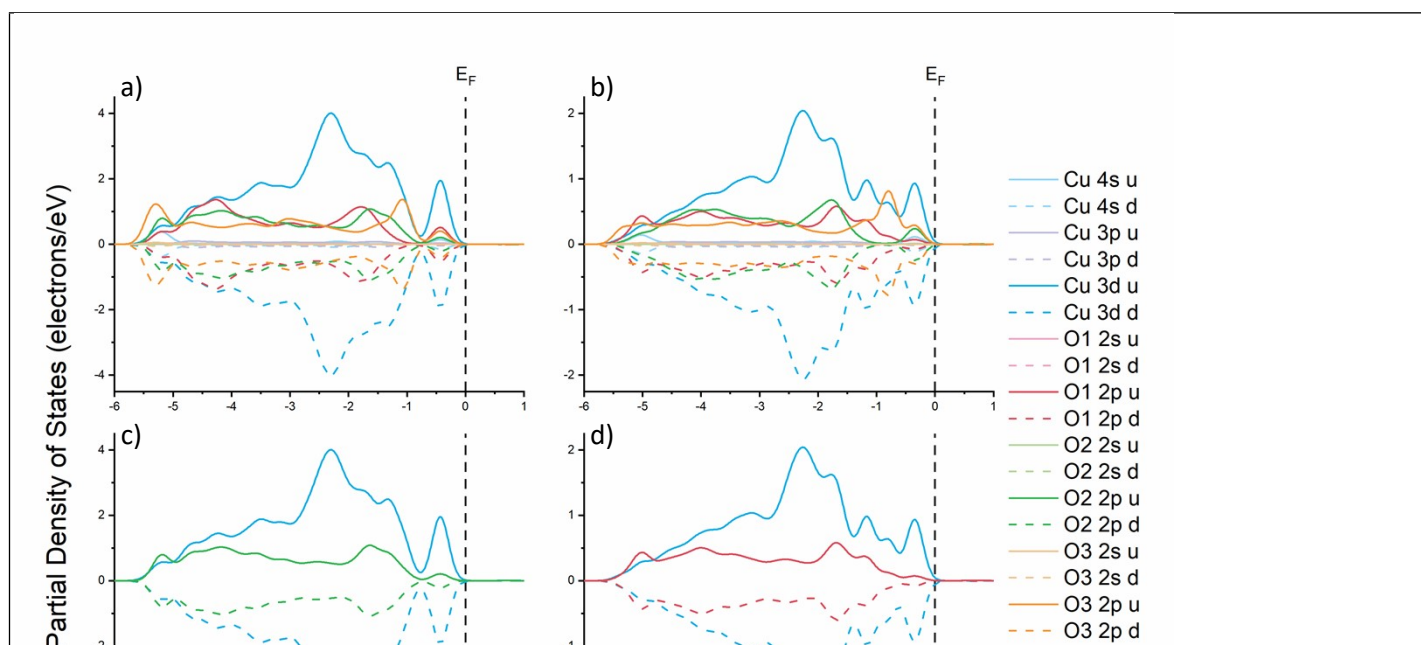
1.2 Adsorption of Cu₂ on CeO₂(110) surface

In the optimised structure of Conf5, Fig. 2, one Cu atom is at a long bridge site, and the other is on top of a surface four-fold hollow site. Since the Cu-O interactions at a four-fold hollow site are much weaker than at a long-bridge site (see ESI Section 1.1), this configuration has a weaker adsorption energy of -2.163 eV, less negative than that of Conf7, 4 and 1. Conf3 shows an optimised structure in which the Cu₂ cluster is almost perpendicular to the surface. This structure is less stable since only the bottom Cu atom is bonded with two surface O ions, showing an adsorption energy of -2.054 eV. In the optimised Conf2, the two Cu atoms are at the same long bridge site, resulting in each Cu being only bonded with one surface O ion from the same long bridge site; since there are no other surface O ions at a bonding distance, it shows the second least negative adsorption energy at -1.725 eV. For Conf6, the two Cu atoms are on top of two second-layer O ions, leading to weak bonding between Cu and surface O ions, thus showing the longest average Cu-O distance of 2.033 Å and the least negative adsorption energy at -0.973 eV.

Conf5 and 6 have two electrons transferred. However, in Conf6, one of the Ce³⁺ ions has a smaller magnetic moment of 0.859 μ_B whose PDOS plot shows a distinct Ce 4*f* signature only partially below E_F (see ESI Fig. 9), while its adjacent Cu₂ cluster has a total magnetic moment of 0.022 μ_B, which together suggest partial reduction of one of the two surface Ce ions. This partial Ce⁴⁺ to Ce³⁺ reduction was also observed in earlier work ².

Conf2 and 3 have only one electron transferred, and they have almost the same Cu₂ total magnetic moment (around 0.33 μ_B, Table 1). However, their retained electron densities are completely different. In Conf2, the retained electron is shared between the two Cu atoms, illustrated by a shared spin density isosurface around the two (see Fig. 2). Cu⁰ has a distinct 4*s* orbital signature below E_F (4*s*¹ state, see ESI Fig. 6), while in Conf2, the two Cu show two similar but much smaller 4*s* signatures partially below E_F (see ESI Fig. 10), indicating again the electron is shared between the two Cu, forming two Cu^{δ+} species, which is also supported by their Bader charges of 0.083 e and 0.169 e, respectively. In addition, the reduced Ce³⁺ ion has a Bader charge of 2.049 e, compared to the average value of 2.292 e of the surface Ce⁴⁺ ions.

In Conf3, Fig. 2.3, both the top and bottom Cu show excess spin density isosurfaces. In the Cu 4*s* and 3*d* PDOS plots, the top Cu atom (ESI Fig. 11, a, c) shows a distinct 4*s* signature around the Fermi energy, and a typical up and down spin 3*d* signatures below E_F. Meanwhile, the bottom Cu (ESI Fig. 11, b, d) hardly shows any 4*s* signature below E_F, but an unoccupied 3*d* signature with a down spin above E_F. The charge density difference isosurfaces, ESI Fig. 12, illustrate charge gain around the top Cu and charge depletion around the bottom Cu. These results together suggest a top Cu^{δ-} and a bottom Cu^{δ+} species, also supported by their Bader charges of -0.059 and 0.474 e, respectively.



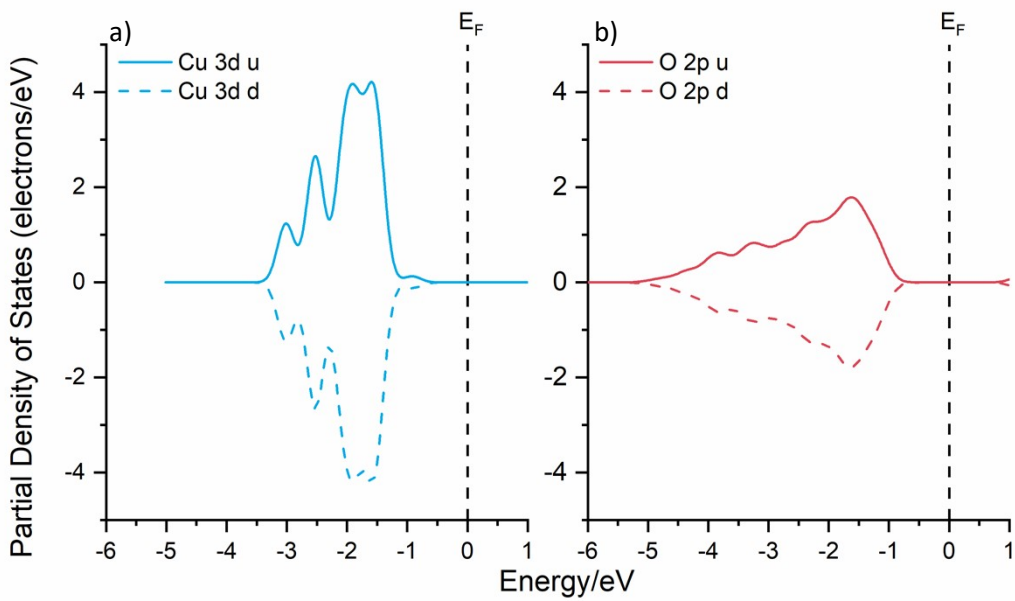


Figure 8: a) Cu 3d PDOS plot of a gaseous Cu_2 dimer; b) O 2p PDOS plot on a pristine $\text{CeO}_2(110)$ surface.

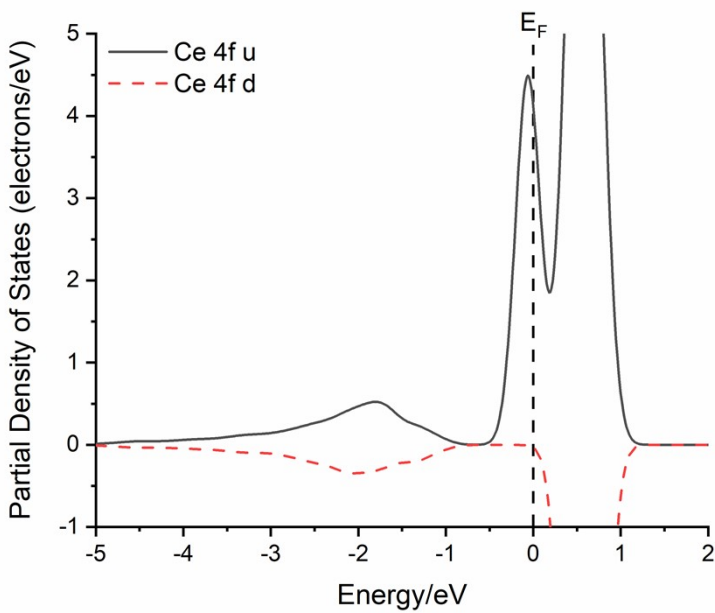
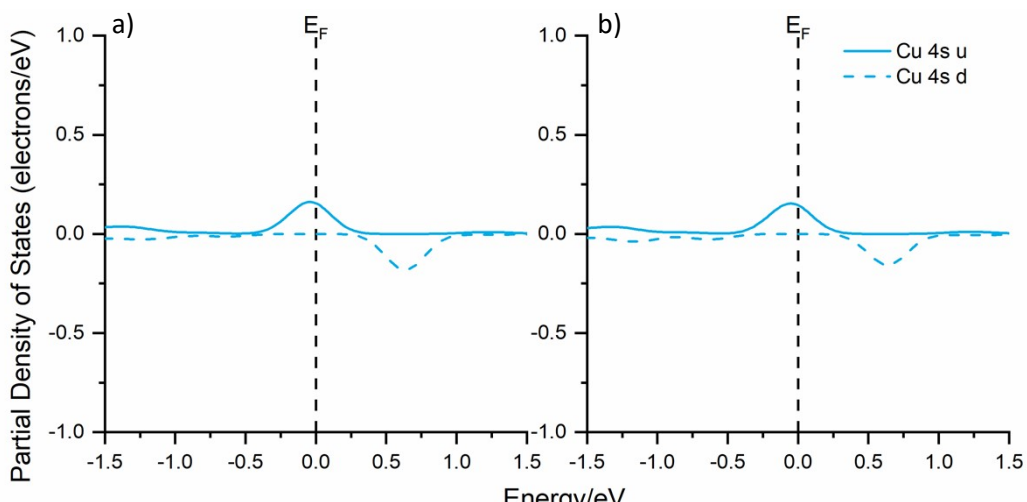


Figure 9: Ce 4f PDOS plot of the partially reduced Ce^{4+} in $\text{Cu}_2/\text{CeO}_2(110)\text{-Conf6}$.



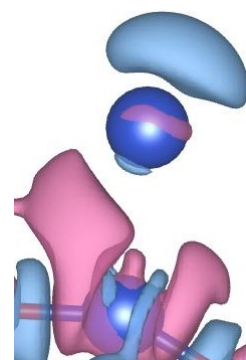
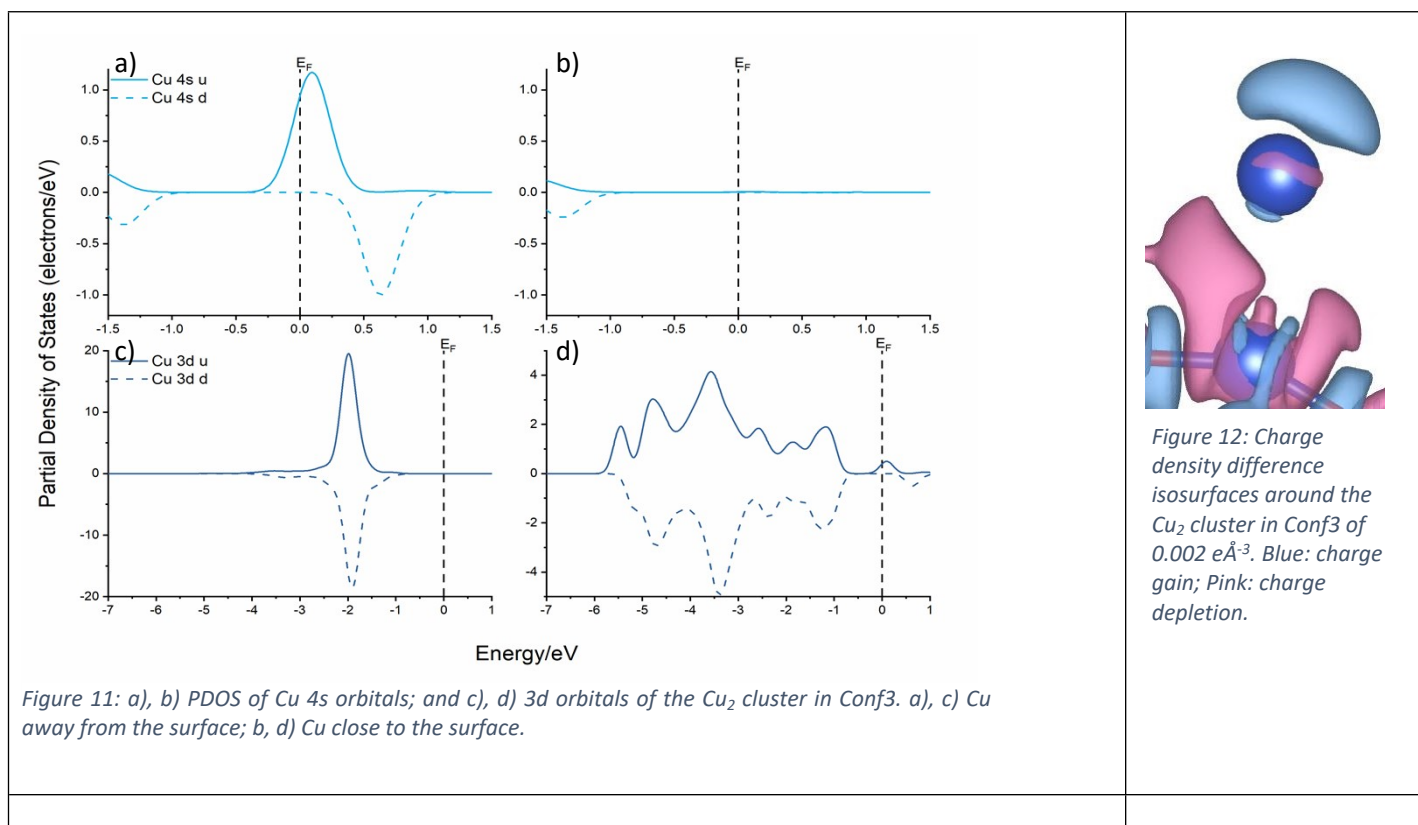


Figure 12: Charge density difference isosurfaces around the Cu₂ cluster in Conf3 of 0.002 eÅ⁻³. Blue: charge gain; Pink: charge depletion.

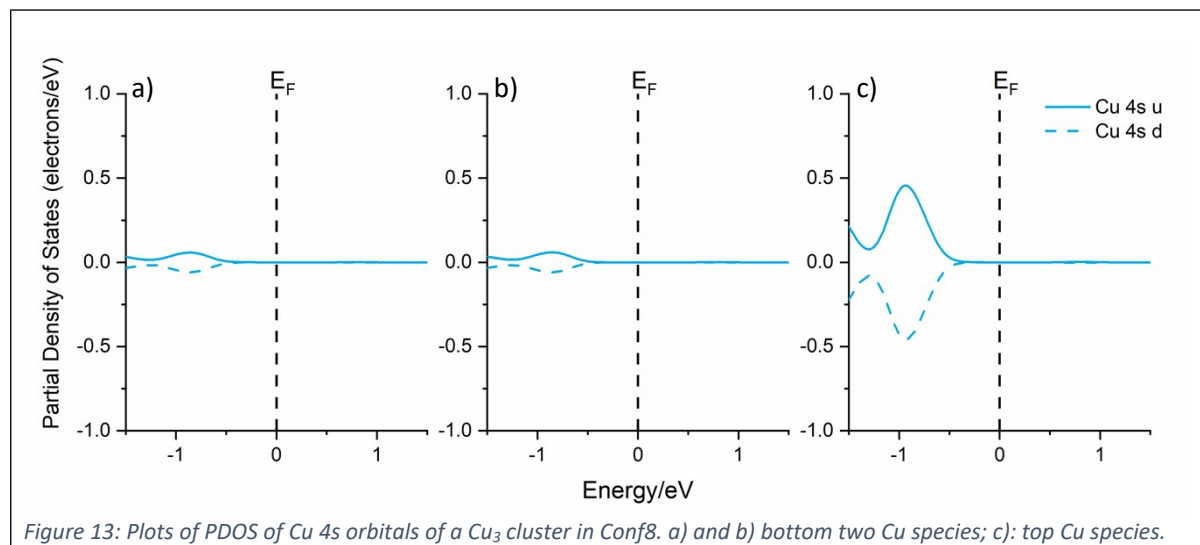
1.3 Adsorption of Cu₃ on CeO₂(110) surface

Both Conf6 and 4 show an elongated Cu₃ triangle, with the third Cu atom bonding with one nearby surface O ion and only one Cu atom, from the initial position at an O_{top} and an O-Ce_{short bdg} site, respectively, resulted from the comparable Cu-O and Cu-Cu interactions. Their Cu adsorption energies, of -2.810 and -2.779 eV, respectively, are weaker than those of Conf3, 2, and 1, since the interactions of the third Cu atom in Conf4 and 6 are not as strong as those in the latter three, in which the third Cu is bonded at a long bridge site.

Conf7, 5, and 8 show the least negative Cu adsorption energies at -2.720, -2.715, and -2.605 eV, respectively. For Conf5 and 8, the third Cu was initially at an O-Ce_{short bdg} and a four-fold_{hollow} site, respectively, with only one or no surface oxygen ions within a bonding distance. Therefore, Cu-Cu interactions surpassed Cu-O interactions, leading to a Cu₃ triangle³ with the third Cu atom away from the surface which bonds only with the bottom two Cu atoms. Conf7 shows an optimised structure essentially the same as that of Conf5 and 8, which however did not change significantly after optimisation. In these three structures, only the bottom two Cu atoms are bonded with surface O ions from two adjacent long bridge sites; the weak copper-surface oxygen interactions, weaker than those in Conf4 and 6, thus result in their least negative adsorption energies.

Interestingly, the Cu₃ total magnetic moment of Conf7, 5, and 8 are zero, suggesting in each case the two retained electrons are spin paired. In the Cu 4s PDOS plots for Conf8, shown in ESI Fig. 13, there are negligible traces of 4s signatures below E_F from the bottom Cu atoms as seen in panels a and b, and two distinct 4s signatures of up and down spins localised on the top Cu atom as shown in panel c, which indicate two bottom Cu⁺ species and a top Cu⁻ species, with the two electrons spin paired in the top Cu⁻ species, which is further shown by the Bader charges of 0.335 and 0.317 e of the bottom two Cu, and -0.179 e of the top Cu. The reduced Ce³⁺ ion shows a Bader charge of 2.074 e, compared to

the average value of 2.305 e of the surface Ce^{4+} ions. A $\text{Cu}^{\delta-}$ species was also reported by Szabová *et al.* when adsorbed on a reduced $\text{CeO}_2(111)$ surface with one oxygen vacancy⁴. Conf5 and 7 show similar electronic structures to Conf8 and thus are not discussed further here.



1.4 Adsorption of Cu_4 on $\text{CeO}_2(110)$ surface

Conf2 shows a roughly linear Cu_4 cluster. The fourth Cu atom is raised above the surface only bridging two nearby bottom Cu atoms at two adjacent long bridge sites, similar to the roughly linear Cu_4 cluster in Conf4; yet, in the latter one, the fourth Cu is bonded with two adjacent Cu atoms as well as surface and second-layer O ions. The weaker Cu-O interactions in Conf2 thus explains its slightly less negative adsorption energy at -2.859 eV.

Conf7 and 8 have adsorption energies at -2.806 and -2.792 eV, respectively. In each configuration, the Cu_4 cluster bonds to two adjacent long bridge sites, showing a Cu_3 triangle connected to the fourth Cu either directly or through an O ion. The three bottom Cu atoms each bond with two surface O ions, whereas the topmost Cu bonds only with one surface O ion. Since the Cu_4 cluster interacts only with the O ions from two long bridge sites, instead of three as in Conf1, 2, 3, and 4, Conf7 and 8 have adsorption energies that are less negative than that of the latter four. Conf6 shows a Cu_4 isosceles trapezium which symmetrically interacts with surface O ions from two adjacent long bridge sites, which leads to much weaker Cu-Cu interactions, compared to those in Conf7 and 8, and thus a less negative adsorption energy of -2.752 eV. Conf5 comprises a Cu_3 cluster and an isolated Cu atom at two adjacent long bridge sites, respectively. Weak Cu-Cu interactions, and weak bonding between the Cu_3 cluster and the surface with only three Cu-O bonds, explain its lowest adsorption energy of -2.470 eV.

Conf7 has an interesting electronic structure for one of the Ce^{3+} ions, whose magnetic moment is -0.755 μ_B with a spin density isosurface in the shape of $4f_{z^3}$, and for the topmost Cu, showing a small spin density isosurface. The PDOS analysis (see ESI Fig. 16) shows a Ce 4f signature partially below E_F , and a Cu 4s signature partially above E_F correspondingly. These together indicate that four electrons are not fully transferred from Cu_4 to the surface, forming a partially oxidised topmost $\text{Cu}^{\delta+}$ species (Bader charge of 0.063 e) and three fully oxidised Cu^+ ions.

Both Conf5 and 6 have two electrons transferred. For Conf5, the two retained electrons are localised around the top two Cu atoms with paired spins, which is evident from PDOS analysis (ESI Fig. 17). Panel

a and b hardly show any observable 4s signatures (-1 to 0 eV), indicating two bottom Cu⁺ ions with Bader charges of 0.484 and 0.448 e, respectively. Both panel c and d show a pair of 4s signatures with opposite spins (-1 to 0 eV), yet the pair in panel d (topmost Cu) shows a much larger magnitude, strongly suggesting a pair of electrons localised around the top two Cu, especially around the topmost Cu, forming a partially reduced topmost Cu^{δ-} and a partially oxidised Cu^{δ+} species. Further evidence is provided by their Bader charges of -0.257 and 0.178 e respectively. However, Conf5 is the least stable structure (0.5 eV less than Conf3), unlikely to be observed in real catalysts. Similarly, Conf6 shows two bottom Cu⁺ ions with Bader charges of 0.519 and 0.311 e respectively, and the top two Cu atoms sharing the two retained electrons in opposite spins (see PDOS plots, ESI Fig. 18). The only difference here is that the electron pair is evenly distributed between the top two Cu, evidenced by their Bader charges of 0.147 and -0.196 e respectively.

From the spin density isosurface plot of Conf4-2, ESI Fig. 19, we note that the two bottom Cu atoms each donates one electron to the surface and the two top Cu share one retained electron, forming two Cu⁺ and two Cu^{δ+} species, also shown by their PDOS plots, ESI Fig. 20. The topmost Cu^{δ+} shows a slightly larger 4s signature below E_F than the other top Cu^{δ+}, suggesting the retained electron moves to the topmost Cu. Interestingly, this retained electron (up spin) is not coupled as in Conf2, yet can be stabilised by the two nearby Ce³⁺ ions (down spin). As a result, Conf4-2 has a similar adsorption energy to that of Conf2, but it is still less stable than Conf4, by 0.12 eV.

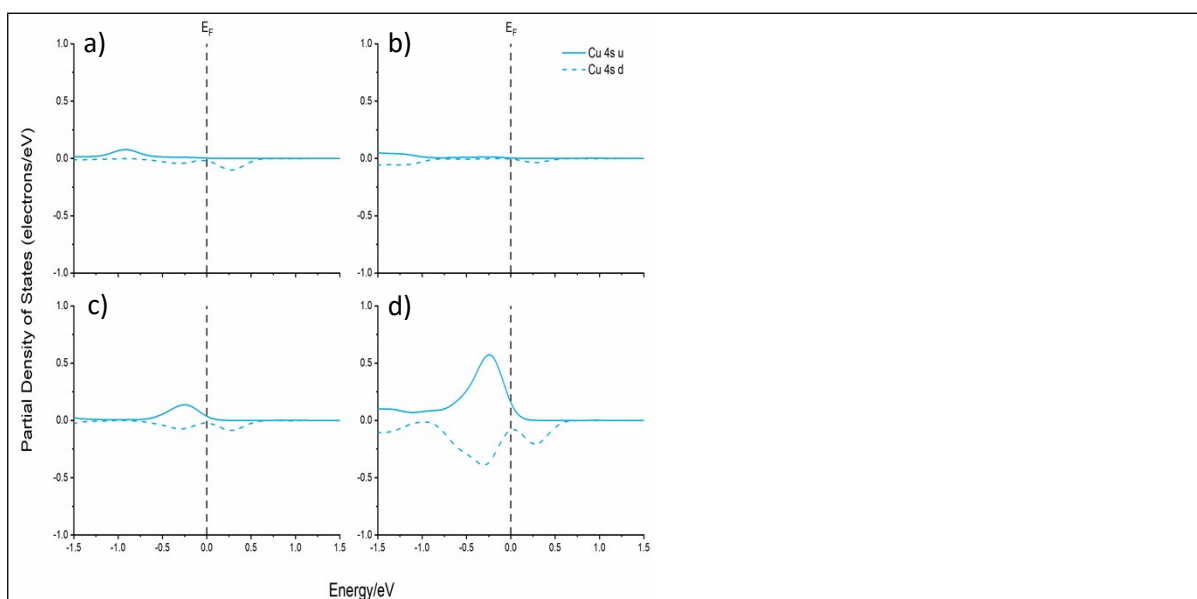


Figure 14: Cu 4s PDOS plots of a Cu₄ cluster in Conf2. a) and b) two bottom Cu species showing spin density in Fig. 6; c) the third bottom Cu species; d) the top Cu species which is furthest away from the surface.

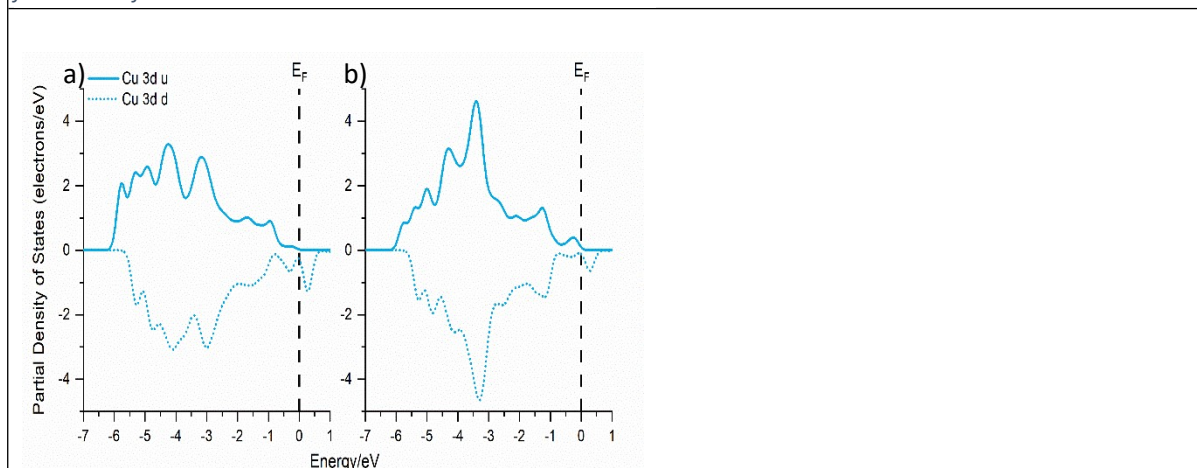


Figure 15: PDOS plots of Cu 3d orbitals of two Cu species in Conf2 with spin density isosurfaces shown in Fig. 6. a) furthest

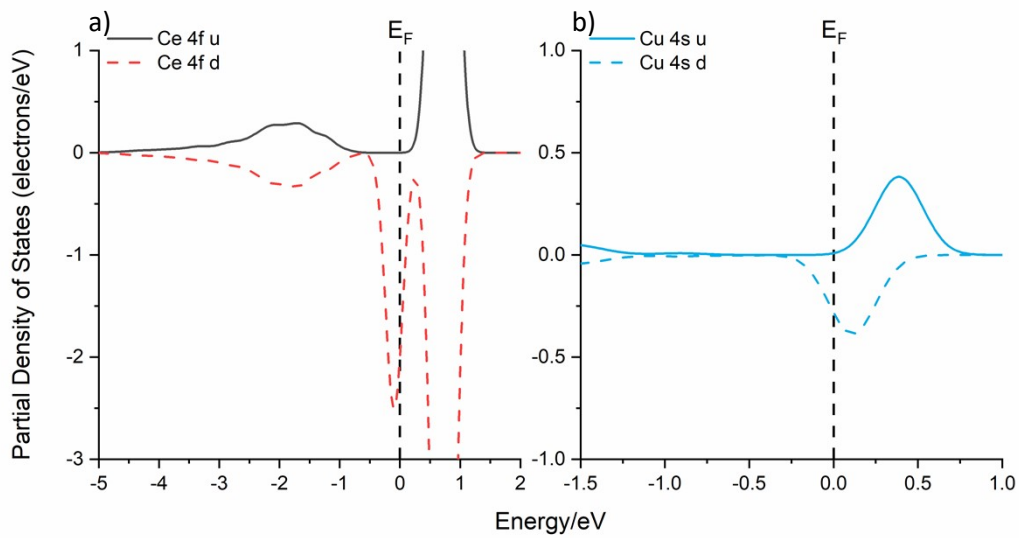


Figure 16: $\text{Cu}_4/\text{CeO}_2(110)\text{-Conf7}$ PDOS analysis. a) Ce 4f orbital PDOS of the partially reduced Ce^{4+} ; b) Cu 4s orbital PDOS of the partially oxidised topmost Cu species.

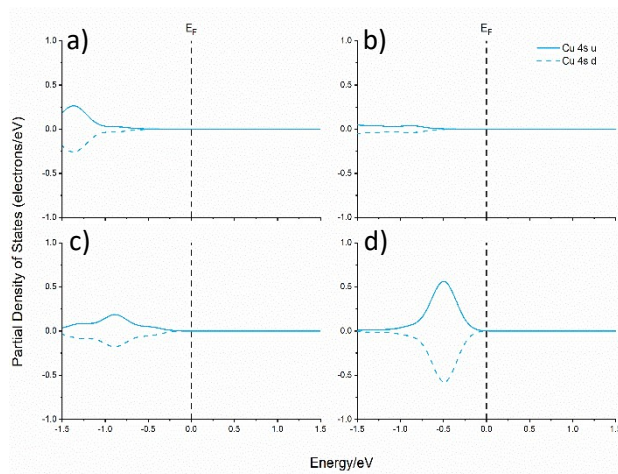


Figure 17: PDOS plots of Cu 4s orbitals of a Cu_4 cluster in Conf5. a) and b) two bottom Cu species shown in Fig. 6; c) and d) two top Cu species; d) is furthest away from the surface.

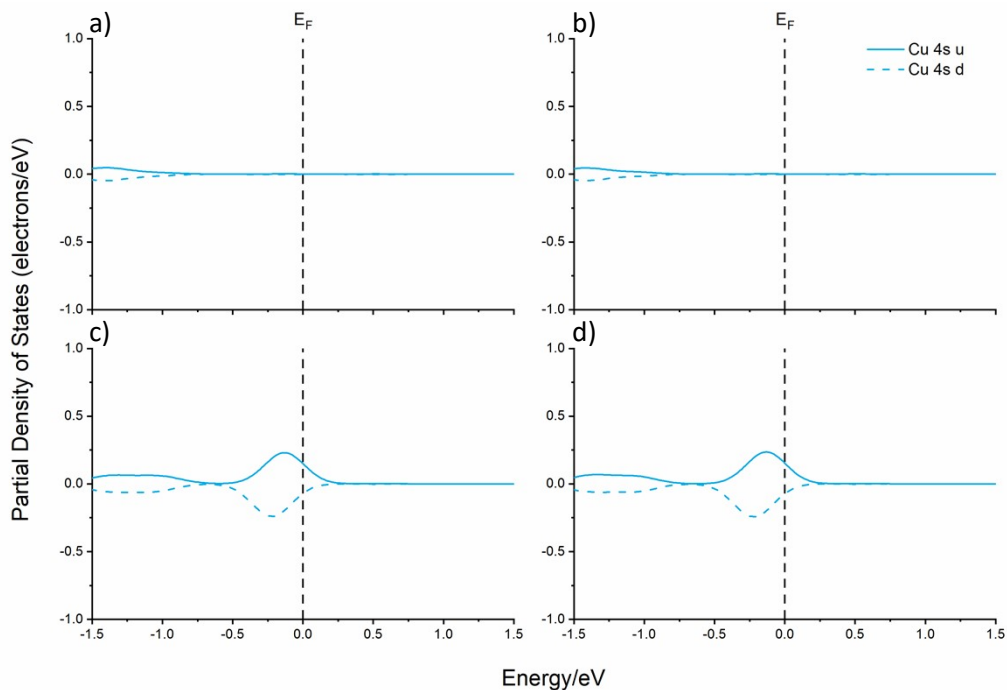


Figure 18: PDOS plots of Cu 4s orbitals of a Cu_4 cluster in $\text{Cu}_4/\text{CeO}_2(110)\text{-Conf6}$. a) and b) two bottom Cu

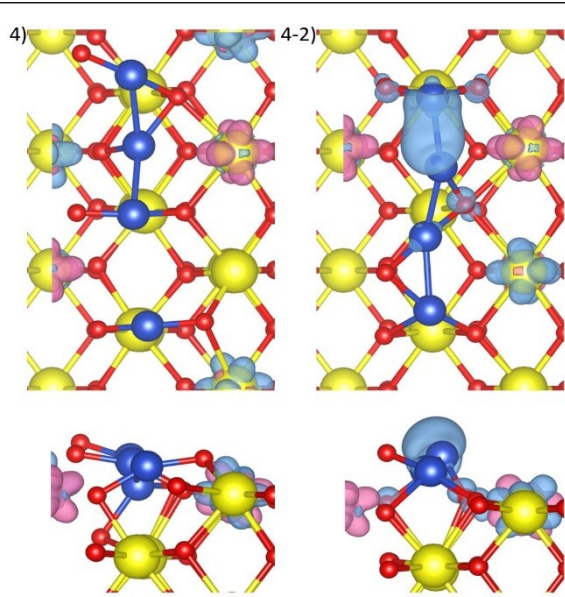


Figure 19: Top and side view of optimised Conf4 and Conf4-2 structures with the spin density isosurfaces of $0.005 \text{ e}\text{\AA}^{-3}$ around Cu and reduced Ce^{3+} ions, labelled as 4) and 4-2).

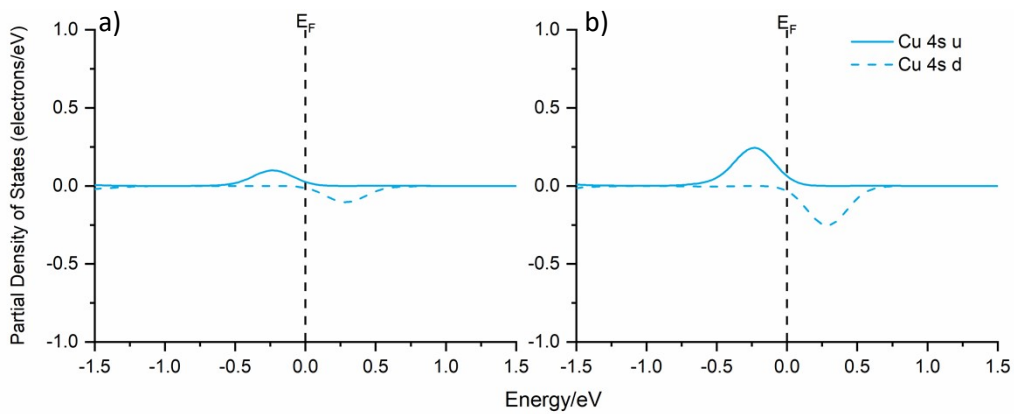
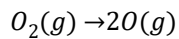


Figure 20: Cu 4s orbital PDOS plots of two Cu showing spin density in Conf4-2, ESI Fig. 19. b) the topmost Cu.

1.5 VASP calculations of O_2 and O atom in the gas phase



The O_2 dissociation energy calculated is as follows.

$$E(\text{O}_2)_{\text{dissociation}} = 2 * (-1.90942784) - (-9.8627076) = 6.04385192 \text{ eV}$$

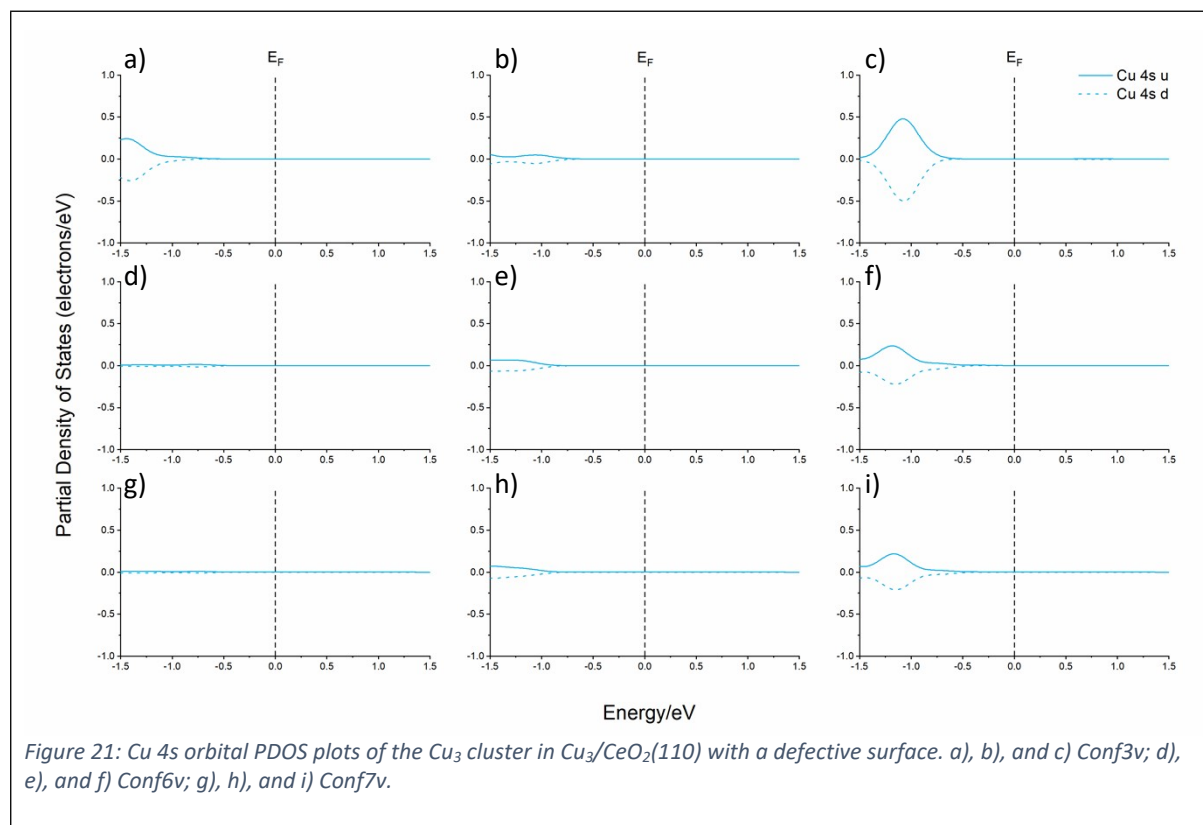
The value calculated by using GGA DFT and PAW potential is close to the experimental value of 5.12 eV as reported in the previous work⁵.

1.6 Adsorption of Cu_3 on $\text{CeO}_2(110)$ surface with one oxygen vacancy

Conf7v and 6v have adsorption energies of -2.575 eV and -2.557 eV, respectively, and show essentially the same optimised structures. However, the optimised Conf6v is very different from that of Conf6 with a stoichiometric surface. The weakened Cu-O interactions due to vacancy formation, and the dominating Cu-Cu interactions cause the third Cu to move away from the surface and bridge the bottom two Cu atoms, forming a standing triangle. The nearest oxygen ion thus does not move close to the vacancy, unlike that found in Conf2v, and therefore a less negative adsorption energy. Significantly weakened Cu-O interactions also caused the third Cu in Conf3v to move away from the surface, bonding with only one bottom Cu atom, therefore leading to the least negative adsorption energy of -2.420 eV. Besides, the Cu₃ cluster in Conf3v is very different from the linear Cu₃ cluster in Conf3 with a stoichiometric surface.

For the latter three configurations, no spin density isosurfaces around the Cu₃ cluster are observed. In Conf7v, there is one surface NN, one surface and one sub-surface NNN. The same Ce³⁺ localisation pattern is observed in Conf6v and 3v. Compared to Conf6v, the two surface Ce³⁺ ions in Conf7v are further apart, which explains its slightly more negative energy than Conf6v. Similar comparisons and results were reported by Kullgren *et al.* when studying different Ce³⁺ pairs on a defective CeO₂(110) surface with one oxygen vacancy ⁶. Although Conf3v shows the same Ce³⁺ localisation pattern as Conf7v, the much weaker Cu-Cu interactions led to its least negative adsorption energy.

The two electrons which are not visible in both spin density isosurfaces and Cu 4s orbital PDOS plots (see ESI Fig. 21) are visualised by the charge density difference isosurfaces, within the Cu₃ cluster (see ESI Fig. 22). For Conf3v, for which the Cu₃ total magnetic moment is zero, the electron pair is localised around the topmost Cu, forming a Cu⁻ species with a Bader charge of -0.316 e, while the bottom two are Cu⁺ ions with Bader charges of 0.465 and 0.209 e. For Conf6v and 7v, the electron pair is shared unevenly between the three Cu atoms, forming two Cu^{δ+} species and one Cu⁰-Cu^{δ-}, as indicated by their Bader charges of 0.353 e, 0.258 e and -0.174 e for Conf6v and 0.364 e, 0.222 e and -0.120 e for Conf7v.



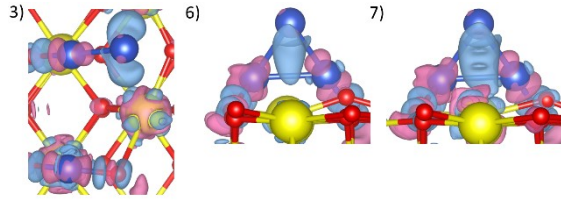


Figure 22: Charge density difference isosurfaces around the Cu₃ cluster in Conf3v (of 0.004 eÅ⁻³), 6v (of 0.003 eÅ⁻³) and 7v (of 0.003 eÅ⁻³) from the Cu₃/CeO₂(110) system with one oxygen vacancy. Blue: charge gain; Pink: charge depletion.

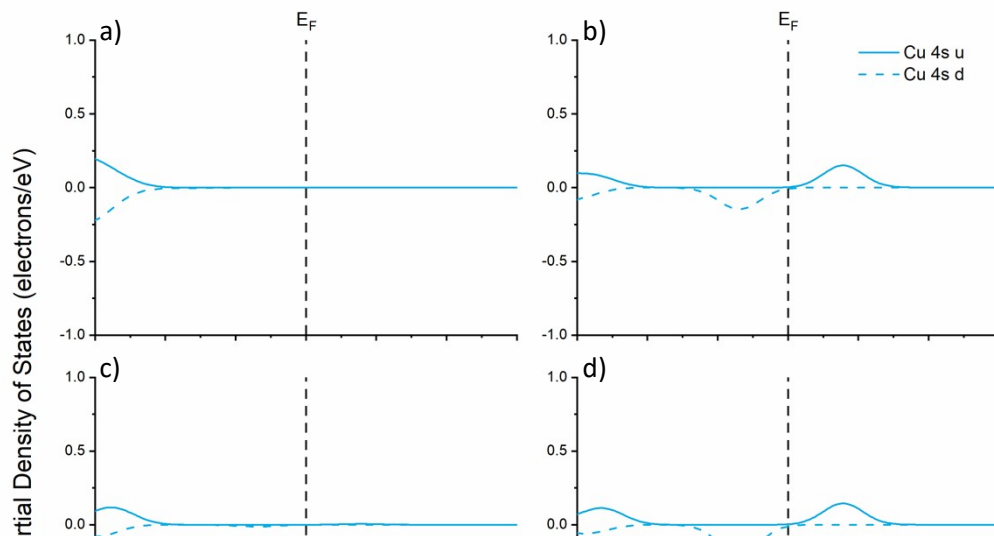
1.7 Adsorption of Cu₄ on CeO₂(110) surface with one oxygen vacancy

Conf2v and 3v have very similar optimised structures, Fig. 11, *i.e.* a standing bonded Cu₃ triangle and an isolated Cu atom at a long bridge site. Weakened Cu-O interactions and relatively stronger Cu-Cu interactions, lead to a Cu₃ triangle plus an isolated Cu in Conf2v, which is very different from the roughly linear Cu₄ cluster in Conf2 with a stoichiometric surface. Conf7v has an optimised structure similar to that of Conf7 with a stoichiometric surface. The four Cu atoms interact strongly with each other, and the cluster bonds to three surface oxygen ions from two adjacent long bridge sites, since one surface oxygen was removed.

In Conf3v, the Cu₃ triangle and the isolated Cu occupy three adjacent long bridge sites, whereas in Conf7v, the Cu₄ cluster only occupies two long bridge sites. The stronger Cu-O interactions in Conf3v explain its slightly more negative adsorption energy of -2.586 eV than Conf7v (-2.574 eV). In Conf2v, the compact localisation of four large Ce³⁺ ions makes it difficult to relax the structure locally, and one Ce⁴⁺ ion is not fully reduced to Ce³⁺ with a magnetic moment of 0.856 μ_B, to which we can attribute the least negative adsorption energy of Conf2v (-2.495 eV).

Conf2v, 3v, and 7v have similar Ce³⁺ localisation patterns, *i.e.* one surface and one second-layer NN to the vacancy, one surface and one second-layer NNN. The two surface Ce³⁺ ions are directly opposite to each other, and the two second-layer Ce³⁺ ions are in the same four-fold hollow site.

For Conf2v, 3v, and 7v, the two electrons that are invisible in Cu 4s orbital PDOS plots (ESI Fig. 24) are visualised by the charge density difference isosurfaces, appearing within the Cu₄ cluster, as shown in ESI Fig. 25. For both Conf2v and 3v, the electron pair is shared within the Cu₃ cluster forming three Cu^{δ+}-Cu⁰ species, while the isolated Cu is fully oxidised to a Cu⁺ ion, which is further shown by their Bader charges of 0.315, 0.243, -0.048, and 0.423 e for Conf2v, and 0.373, 0.214, -0.128, and 0.441 e for Conf3v. For Conf7v, the electron pair appears around the two middle-layer Cu atoms, forming three Cu^{δ+}-Cu⁰ species and one Cu⁺ ion, with Bader charges of 0.254, 0.189, -0.092, and 0.442 e, respectively.



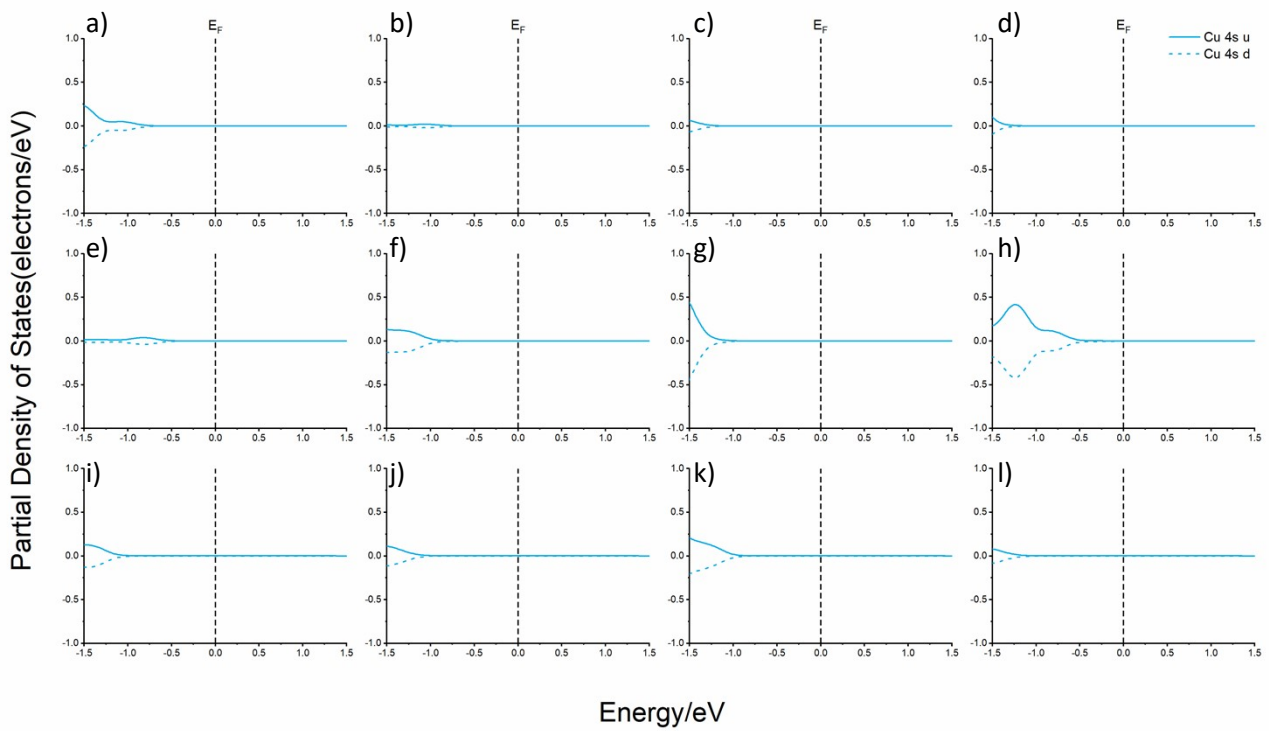


Figure 24: Cu 4s orbital PDOS plots of the Cu_4 cluster in $\text{Cu}_4/\text{CeO}_2(110)$ with a defective surface. a), b), c), and d) Conf2v; e), f), g), and h) Conf3v; i), j), k), and l) Conf7v.

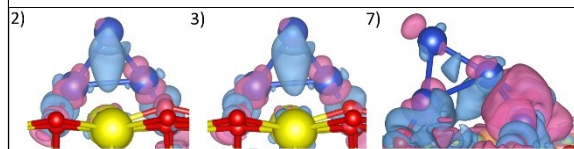


Figure 25: Charge density difference isosurfaces around the Cu_4 cluster in Conf2v (of $0.003 \text{ e}\text{\AA}^{-3}$), 3v (of $0.003 \text{ e}\text{\AA}^{-3}$) and 7v (of $0.0025 \text{ e}\text{\AA}^{-3}$) from the $\text{Cu}_4/\text{CeO}_2(110)$ system with one oxygen vacancy.

Table 2: Calculated magnetic moment of Ce³⁺ ions (s, p, d, f orbitals) in Bohr magneton (μ_B); adsorption energy per Cu atom (eV) of structures showing either ferromagnetic or antiferromagnetic behaviours.

	Ferromagnetic		Antiferromagnetic	
	M_{Ce} (μ_B)	E_{ad} (eV)	M_{Ce} (μ_B)	E_{ad} (eV)
Cu₂/CeO₂(110)				
Conf1	0.942, 0.969	-2.809	0.940, -0.969	-2.810
Conf2	0.965, Cu(0.329)	-1.725	--	--
Conf3	--	--	-0.968, Cu(0.326)	-2.054
Conf4	0.965, 0.964	-3.356	0.966, -0.964	-3.367
Conf5	0.953, 0.953	-2.162	0.952, -0.953	-2.163
Conf6	--	--	0.859, -0.965	-0.973
Conf7	--	--	-0.966, 0.968	-3.492
Cu₃/CeO₂(110)				
Conf1	--	--	-0.967, 0.969, 0.972	-3.307
Conf2	--	--	-0.964, 0.970, 0.973	-3.318
Conf3	--	--	0.960, -0.971, 0.967	-3.429
Conf4	0.962, 0.940, 0.966	-2.611	0.965, -0.967, -0.934	-2.779
Conf5	--	--	0.968	-2.715
Conf6	0.954, 0.939, 0.963	-2.627	0.963, -0.958, -0.968	-2.810
Conf7	--	--	0.967	-2.720
Conf8	0.963, 0.970,	-2.468	0.964	-2.605
Cu₄/CeO₂(110)				
Conf1	--	--	-0.961, -0.958, 0.958, 0.952	-2.918
Conf2	--	--	-0.966, 0.967, -0.954	-2.859
Conf3	--	--	0.945, 0.966, 0.965, -0.951	-2.971
Conf4	--	--	0.970, -0.964, 0.967, -0.964	-2.961
Conf4-2	--	--	0.969, -0.950, -0.963	-2.840
Conf5	--	--	0.964, -0.968	-2.470
Conf6	--	--	0.949, -0.969,	-2.752
Conf7	--	--	-0.755, -0.971, 0.966, 0.969	-2.806
Conf8	0.968, 0.943, 0.962, 0.962	-2.798	0.958, -0.942, 0.957, -0.963	-2.792
CeO₂(110)-Ov				
Case1	0.958, 0.958	1.542	0.969, -0.973	1.110
Case2	0.961, 0.897	1.431	0.962, -0.898	1.426
Case3	--	--	-0.966, 0.945	0.978
Cu/CeO₂(110)-Ov				
Case1	0.969, 0.955, 0.973	-3.595	--	--
Case2	--	--	0.968, 0.971, -0.967	-3.690
Cu₂/CeO₂(110)-Ov				

Conf1	--	--	-0.975, -0.971, 0.967, -0.959	-3.356
Conf4	--	--	-0.973, -0.970, -0.951, 0.963	-3.207
Cu ₃ /CeO ₂ (110)-Ov				
Conf1v	--	--	0.975, 0.975, -0.969, -0.960, -0.964	-3.348
Conf2v	--	--	0.975, -0.976, 0.969, 0.962, 0.964	-3.350
Conf3v	--	--	0.969, 0.968, -0.968	-2.420
Conf6v	--	--	-0.972, 0.969, 0.952	-2.557
Conf7v	0.971, 0.968, 0.950	-2.575	--	--
Cu ₄ /CeO ₂ (110)-Ov				
Conf2	--	--	-0.973, 0.968, 0.857, -0.955	-2.495
Conf3	0.958, 0.967, 0.948, 0.960	-2.588	-0.968, 0.967, 0.952, -0.953	-2.586
Conf4	--	--	-0.974, 0.966, 0.962, -0.964, -0.960	-2.674
Conf7	0.958, 0.965, 0.954, 0.946	-2.397	0.952, 0.972, -0.968, -0.962	-2.574

Table 3: Investigation of the adsorption energy per Cu atom (eV) of the most stable structures including the van der Waals forces using DFT+U+D3.

System	E_{ad} (eV)	
	DFT+U	DFT+U+D3
Cu/CeO ₂ (110) O _{top}	-3.258	-3.483
Cu ₂ /CeO ₂ (110) Conf7	-3.492	-3.595
Cu ₃ /CeO ₂ (110) Conf3	-3.429	-3.581
Cu ₄ /CeO ₂ (110) Conf3	-2.971	-3.076
Cu ₄ /CeO ₂ (110) Conf4	-2.961	-3.170
Cu/CeO ₂ (110)-Ov case2	-3.690	-3.695
Cu ₂ /CeO ₂ (110)-Ov Conf1v	-3.356	-3.446
Cu ₃ /CeO ₂ (110)-Ov Conf2v	-3.350	-3.392
Cu ₄ /CeO ₂ (110)-Ov Conf4v	-2.674	-2.805

2. References

1. Chutia, A.; Gibson, E. K.; Farrow, M. R.; Wells, P. P.; Scanlon, D. O.; Dimitratos, N.; Willock, D. J.; Catlow, C. R. A., The adsorption of Cu on the CeO₂(110) surface. *Phys Chem Chem Phys* **2017**, *19* (40), 27191-27203.
2. Cui, L.; Tang, Y.; Zhang, H.; Hector, L. G., Jr.; Ouyang, C.; Shi, S.; Li, H.; Chen, L., First-principles investigation of transition metal atom M (M = Cu, Ag, Au) adsorption on CeO₂(110). *Phys Chem Chem Phys* **2012**, *14* (6), 1923-33.
3. Ren, Z.; Liu, N.; Chen, B.; Li, J.; Mei, D., Nucleation of Cu_n (n = 1–5) Clusters and Equilibrium Morphology of Cu Particles Supported on CeO₂ Surface: A Density Functional Theory Study. *The Journal of Physical Chemistry C* **2018**, *122* (48), 27402-27411.
4. Szabová, L.; Camellone, M. F.; Huang, M.; Matolin, V.; Fabris, S., Thermodynamic, electronic and structural properties of Cu/CeO₂ surfaces and interfaces from first-principles DFT+U calculations. *J Chem Phys* **2010**, *133* (23), 234705.
5. Ruscic, B.; Feller, D.; Peterson, K. A., Active Thermochemical Tables: dissociation energies of several homonuclear first-row diatomics and related thermochemical values. *Theoretical Chemistry Accounts* **2013**, *133* (1).
6. Kullgren, J.; Hermansson, K.; Castleton, C., Many competing ceria (110) oxygen vacancy structures: from small to large supercells. *J Chem Phys* **2012**, *137* (4), 044705.